Flow Dynamics and Stability in a Severe Rainband

G. CHIMONAS AND G. KALLOS*

School of Geophysical Sciences, Georgia Institute of Technology, Atlanta, GA 30332

(Manuscript received 13 March 1985, in final form 6 February 1986)

ABSTRACT

Observations of a severe form of rainband, which is comprised of a line of strong but shallow convection, suggest that the environment into which it moves is nearly neutrally stratified with respect to moist convection. A simple two-dimensional model of a severe rainband has been developed to explore how the cold air at the base of the rainband modifies local stability as it underruns the saturated surface layer. This dynamic lifting is found to have two distinct effects. First, the lifted fluid contains regions of absolute and conditional instability. Then it also reorganizes the midtroposphere into a sequence of elevated inversions set between unstable layers. This latter effect results from the intense "lee wave" response in the air flow. The elevated inversions would appear to cap the severe moist convection, establishing the rainband character rather than allowing the deep cellular convection of squall lines. The flow disturbances end abruptly at the steering level (a critical level for the waves), which appears to define the upper limit of the rainband activity.

1. Introduction

Organized systems of severe convection are frequently associated with currents of cold surface air. In this paper we examine the changes in stability characteristics that follow the tropospheric adjustment to the presence of these surface currents. The calculation has much in common with the lee wave problem, although in the present case the lowest part of the troposphere is saturated with water vapor, and the sharp head of the cold air current prevents the use of a linearized response formulation near the surface.

The work is presented entirely in the context of severe rainbands in a marine-type environment, and calculations are made for one such set of field observations. However, the concepts and numerical techniques may be readily modified to study flows in gust fronts and perhaps even squall lines.

Figure 1 illustrates the physical system. A tongue of cold dense air flows under a saturated surface layer that feeds into a line of severe shallow convection. The mature system is essentially two-dimensional and will be modeled as such. Our aim is to discover how the intrusion of the cold air releases the energy stored as latent heat in the saturated layer and otherwise affects the evolution of the environment. We seek to obtain a good shape for the head of the cold air flow and a reliable solution for the air motion above it.

Two models are studied, both being essentially stable in the upstream region. The first consists of a simple inflow system that tests the procedures, providing results that are credible, if somewhat unexciting. This first inflow field is not representative of rainband conditions as it excludes a steering level. In the lifted region it predicts potential instability that would normally be associated with deep cellular convection.

The second inflow used is, by contrast, modeled from field data. It introduces certain dynamical complexities into the calculation. But more importantly it yields results that are totally distinct from the first. Potential instability is found in a relatively shallow layer above the head of the cold air mass. But, above this a complex structure extends through the midtroposphere, alternating layers of instability with elevated inversions. The activity ends abruptly at the steering level, above which the flow retains its undisturbed upstream characteristics. This height is coincident with the observed upper level of the rainband activity.

These results are consistent with the concept that the severe moist convection in a rainband is forced by the underflow of cold surface air and localized by the dynamic response of the midtroposphere.

2. The rainband environment

Field studies of severe rainbands have revealed a variety of definite characteristics (Carbone, 1982; Moore, 1984; Hobbs and Persson, 1982; references contained therein). The severe narrow rainband appears as a line-like region of severe but shallow convection without apparent cellular substructure. The line of severe activity may be some hundreds of kilometers long but only ten or so kilometers across, and it is confined to a lower region of the troposphere. Such events occur in marine dominated environments. The land ahead

* Permanent affiliation: University of Athens, GA.

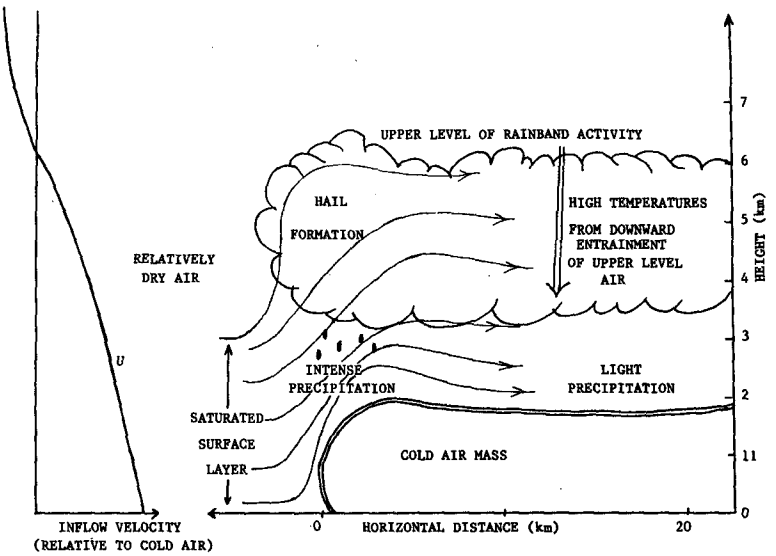

FIG. 1. Schematic of the rainband. The cold air current wedges beneath the saturated boundary layer. A line of severe but shallow convection occurs above the head of the surface intrusion.

of the line is covered with a deep saturated layer of surface air, while the surface air behind the line is relatively cold. Soundings in the undisturbed region well ahead of the line show little or no sign of instability, meaning that a tephigram plot reveals essentially no positive area for lifting.

This paper is concerned with the stability of the troposphere in the immediate vicinity of a band. We will use data obtained in Carbone's case study, which involved a line of severe storm activity that passed through a field site in Northern California. Stability characteristics of this event agree with those reported by Hobbs and Persson for more northerly events, and earlier work performed in Europe, indicating that the characteristics are a general feature of these events.

Figure 2, taken from Carbone's study, shows that the atmosphere ahead of the rainband is almost neutrally stable in the sense that the diagram has essentially no positive area for a parcel lifted from the surface. Severe convective activity, which occurs within the rainband, requires local stability characteristics much different from those seen in this upstream region. Yet the rainband propagates into this environment and thrives. The primary motivation of this study is to discover how this can be so—how the local stability conditions required for severe convection can develop from the seemingly unsupportive air mass ahead of it. Further, we address the question of why the severe convection should be shallow and continuous, as distinct from the lines of deep cells found in squall lines.

The present calculation models the environment that results as the saturated surface layer rises over the cold current traveling with the rainband. This model environment differs from the field that occurs at the site of the meteorological activity as the calculations do

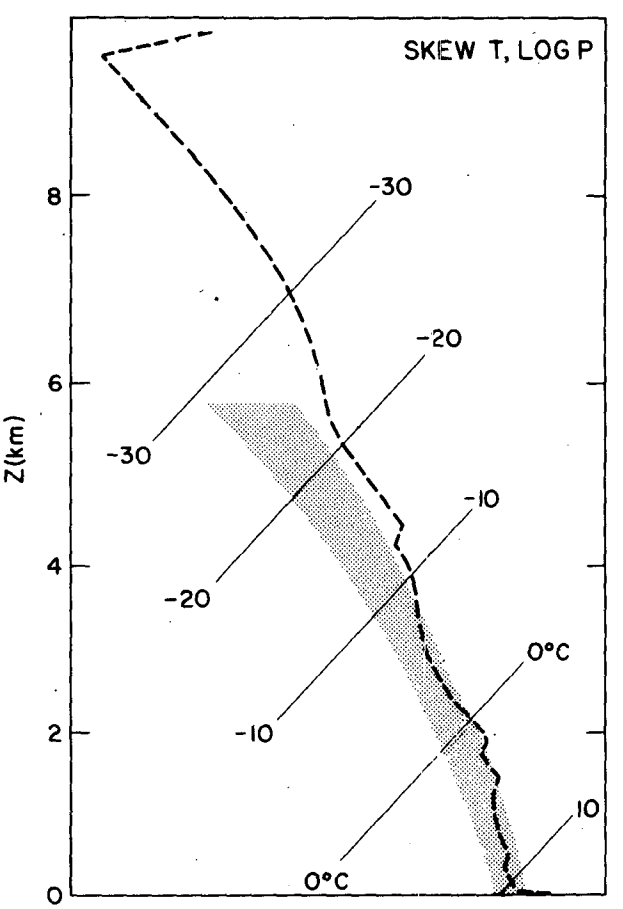

FIG. 2. Sounding in the air ahead of a rainband. The stippled area covers the extreme range of pseudo-moist adiabats available to boundary layer air. There is very little potential for convective activity (from Carbone, 1982).

not include the storm activity. However, there should be a reasonable correlation between the unstable locations predicted by our model and the observed locations of the storms. Moreover, the degree of instability found in the model provides a guide to the expected storm severity.

3. The model and its equations

Field observations lead to a characteristic shape for the surface cold air current. Schematics such as Fig. 3 are currently in use. Our model takes the general features of this shape as given and also assumes other characteristics such as its speed of propagation. Thus we are not investigating the characteristics of the surface cold air flow at all. We are concentrating on the response of the moist layer of surface air as it is lifted by the cold intrusion.

Figures 4 and 5 show sets of upstream conditions that will be used in our calculations. A deep, saturated layer adjacent to the surface is topped by stable air with rather low relative humidity. There is no static instability of any type in these upstream profiles. The low relative humidity in the upper air allows us to treat it as a perfect gas—no phase changes will occur there. The flow contains wind shear and a temperature structure that merges into an uppermost flow with constant wind and stratification. This allows a relatively simple form for the upper boundary conditions.

In the calculations, the flow in the saturated lower layer is given a nonlinear (but laminar) treatment. The formulation adopted follows that given by Lilly (1979) for wet air in which the water undergoes phase changes. For details of the full general formulation the reader is referred to Lilly's paper, specifically sections 1 and 3. However, conditions in the rainband environment

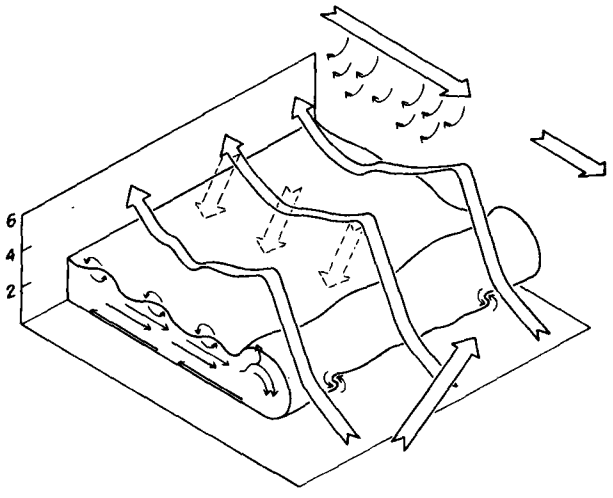

FIG. 3. Structure of the cold air density intrusion and the overflowing warm air (from Carbone, 1982). Such forms are deduced from radar data.

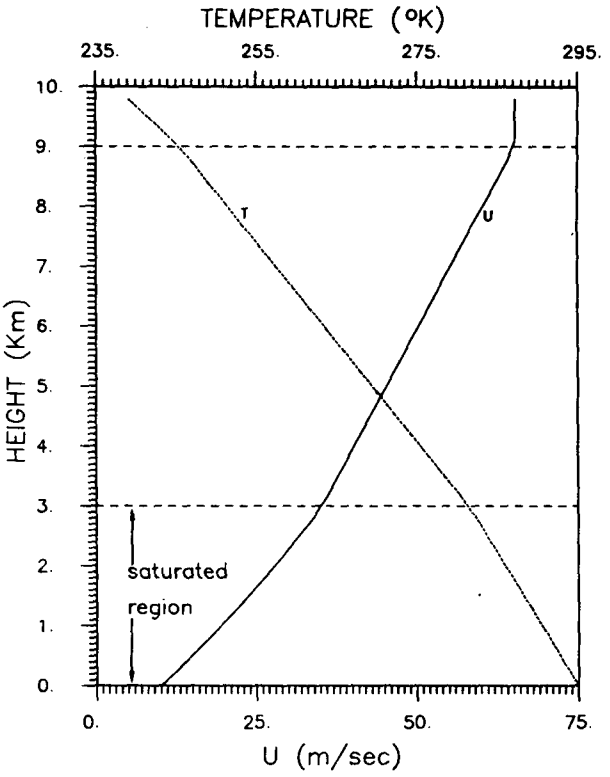

FIG. 4. Inflow temperature and wind used in the first set of model calculations. Unless otherwise stated, results presented for this model derive from this particular profile set.

are quite special and our calculations only need a special form of Lilly's formula. This form is readily obtained from the basic equations governing the fluid; we present its derivation in the Appendix. We reference the general formulation as it gives a broader context to the approximations adopted.

The formulation is simplified by the occurrence of constant equivalent potential temperature θ_e through the moist layer. This condition is seen in the soundings taken ahead of the line of severe weather and may be expected in humid prestorm surface layers that have evolved through convective overturning and mixing.

The calculations are performed in the frame of reference that moves with the cold air intrusion, and it is assumed that the entire system is stationary and two-dimensional. The upstream flow characteristics are specified at the outset. The intention is to discover the streamlines and thermodynamic properties throughout the lifted air mass. No attempt will be made to model properties within the cold intrusion, the bounding shape of which is obtained indirectly (section 4) but conforms with observations.

The rise over the leading edge of the intrusion is both large and sudden. Consequently a linearized treatment of the simpler lee wave variety is inappropriate; instead, the saturated layer requires a nonlinear treatment. The flow in the upper layer is given the less

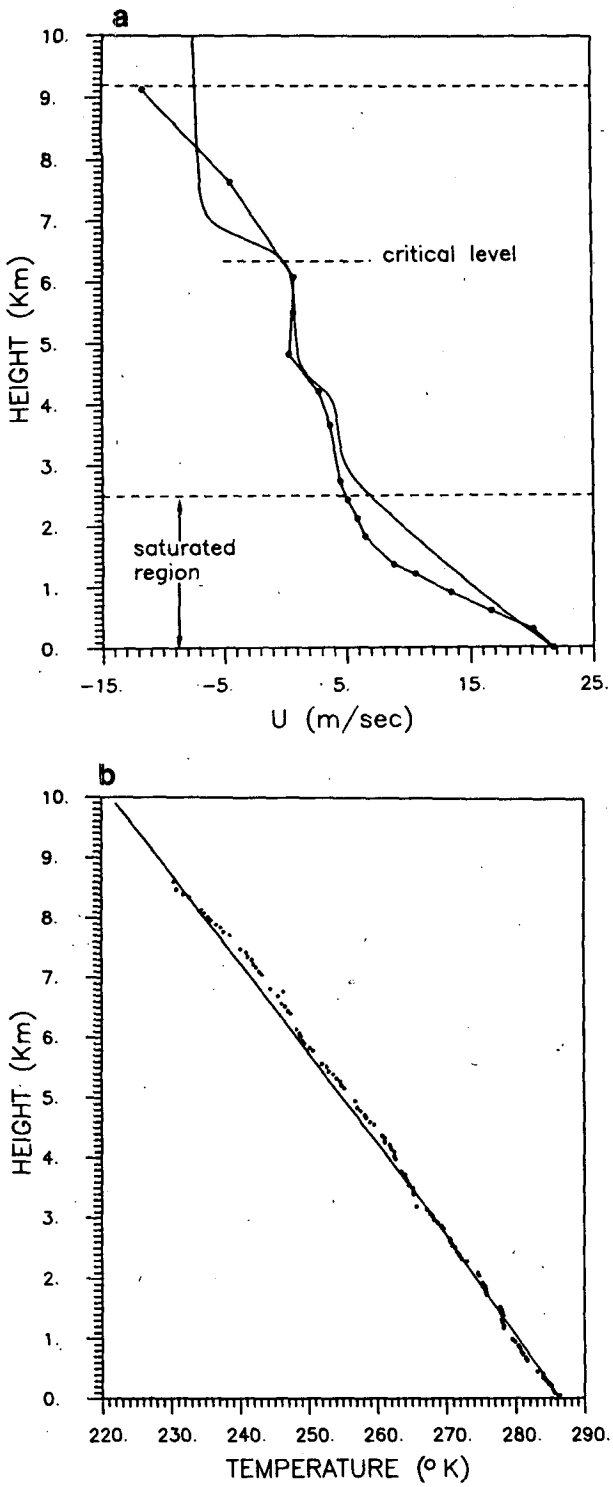

FIG. 5. Inflow profiles derived to model rainband data reported by Carbone (1982). Dots are rawinsonde values. (a) Wind in rest frame of rainband; (b) temperature.

exact linearized formulation, anticipating that the thick humid layer shields the upper fluid from the more abrupt components of the displacement. Then disturbances and matching conditions at the upper face of the saturated layer may be treated with linearized theory. Boundary conditions in the upper region are the familiar lee wave conditions (Appendix). When the streamlines have been obtained, the thermodynamic fields are readily deduced.

A stationary, wet, two-dimensional adiabatic flow can be described in terms of a mass-weighted streamfunction ψ (Lilly, 1979)

$$\rho u = \frac{\partial \psi}{\partial z}, \quad \rho w = -\frac{\partial \psi}{\partial x}, \tag{1}$$

$$\frac{1}{\rho}\nabla\cdot\left(\frac{1}{\rho}\nabla\psi\right) = \frac{1}{\rho_0}\frac{du_0}{dz_0} + (c_p/\theta_e)\frac{d\theta_e}{dz_0}\frac{(T_0 - T)}{\rho_0 u_0} \tag{2}$$

where ρ is mass density, u and w are the horizontal and vertical components of velocity, respectively, θ_e is equivalent potential temperature, T the kinetic temperature and c_p the specific heat of air at constant pressure. A subscript "0" denotes evaluation on the streamline (ψ = constant) at its inflow location ($x = \infty$).

Throughout the lower fluid, θ_e is constant, so

$$\frac{1}{\rho}\nabla\cdot\left(\frac{1}{\rho}\nabla\psi\right) = \frac{1}{\rho_0}\frac{du_0}{dz_0}, \tag{3}$$

an equation that is much simpler than the general form (2).

Density perturbations are usually of little significance in the dynamics of low-frequency flows, so $\rho(x, z)$ in the left-hand side of (3) is replaced by a mean density function $\bar{\rho}(z)$;

$$\frac{1}{\bar{\rho}}\nabla\cdot\left(\frac{1}{\bar{\rho}}\nabla\psi\right) = \frac{1}{\rho_0}\frac{du_0}{dz_0} = F(\psi). \tag{4}$$

The right-hand side of this equation is generally a function of both x and z. It defines the advected characteristics of the flow (i.e., it maintains a constant value along a streamline). The equation simplifies enormously when this function becomes a global constant of the layer

$$\frac{1}{\rho_0}\frac{du_0}{dz_0} = \text{constant} = q. \tag{5}$$

In this limit we can also derive the equation for the streamline in a simple direct manner from the basic equations of motion. This is demonstrated in the Appendix. However, the relation to the more general form (2) sets the calculation in its broader context.

In the limit given by (5), Eq. (4) may be solved by a partition of ψ:

$$\left.\begin{aligned}\psi &= \bar{\psi} + \psi_1(x, z)\\ \bar{\psi} &= \psi_0(z_0 = z)\end{aligned}\right\}, \tag{6}$$

$$\left(\frac{1}{\bar{\rho}}\right)\nabla\cdot\left(\frac{1}{\bar{\rho}}\nabla\psi_1\right) = 0, \tag{7}$$

$$\frac{d}{dz}\left(\frac{1}{\rho_0}\frac{d}{dz}\psi_0\right) = \rho_0 q. \tag{8}$$

Equation (7) is a simple linear second-order differential equation, but it describes a highly nonlinear flow field!

In the unsaturated layer standard linearized theory is used. With modern numerical codes there is no necessity for further approximations. However, the differences between results of the fully compressible formulations and those that ignore compressibility except in stratification effects are usually minimal—smaller than differences that arise within one formulation when the background winds and temperatures are varied slightly. Consequently, the simplified theory, which is certainly easier to formulate, is adopted. Accordingly, the streamfunction in this region is the sum of an undisturbed part plus a perturbation ψ_1 that obeys the equation (Appendix):

$$\left(\frac{\partial^2}{\partial x^2} + \frac{\partial^2}{\partial z^2}\right)\psi_1 - (\rho_0'/\rho_0)\frac{\partial}{\partial z}\psi_1 + \left(\frac{N^2}{U^2} - \frac{U''}{U}\right)\psi_1 = 0 \tag{9}$$

where U is the mean horizontal velocity, a prime denotes a derivative with respect to z, and N is the Brunt-Väisälä frequency,

$$N^2 = g\left[\frac{(\gamma - 1)g}{C^2} + \frac{T'}{T}\right].$$

The boundary conditions at the interface of the two fluid layers are that ψ_1 and p (pressure) must be continuous. At the upper boundary of the model the solution must either decay exponentially or have upwards directed group velocity, since all disturbances originate in the lower atmosphere (Appendix). And finally (but fundamentally) the flow at the base of the wet layer must follow the contour defined by the cold air intrusion, and upstream of this, the ground.

4. Formulation of the solution

The flow field in the lifted air mass is derived from the equation set specified in section 3, and three sets of boundary conditions. The first set, the upper-altitude boundary conditions of the usual lee wave type, has already been mentioned. Next, there is the inflow field, to be chosen for model purposes or to be fitted to data obtained ahead of the event. The final set is the surface shape—the physical lower boundary defined by the cold air intrusion and the ground ahead of it. We have adopted an indirect technique here that greatly simplifies the calculation. In a direct approach, the surface shape would be specified at outset. But this shape is known only in a schematic fashion—indeed there may not be any one shape but rather a whole class of allowed shapes. We choose to work within this indeterminacy. Instead of specifying a shape at the outset, we use a procedure that provides both solution and lower boundary shape as output. Representations of the surface current, such as Fig. 3, are defined only within two parameters—the depth of the cold air mass, and the distance over which it is established. The shape also has some obvious qualitative characteristics—it is steplike with some overshoot or bulge in the head region. Our solution contains these general characteristics. But it is obtained indirectly by specifying the streamfunction $\psi_1(x, z)$ of (7) on the plane $z = 0$. Thus we specify

$$\psi_1(x, 0) = A \tanh(x/h) \tag{10}$$

which completes the mathematical boundary conditions for a unique solution throughout all space. Now we can solve the equations to find the full streamfunction (6):

$$\psi = \psi_1(x, z) + \psi_0(z).$$

The lower surface of the saturated air mass is given by the streamline (x_s, z_s) that starts at the ground, far upstream. That is, (x_s, z_s) is defined implicitly by

$$\psi_1(x_s, z_s) + \psi_0(z_s) = \text{constant} = \psi_1(-\infty, 0) + \psi_0(0). \tag{11}$$

This streamline defines the shape of the cold air mass, since the saturated air mass rests either on the ground (the upstream region) or on the intruding cold air. Its shape is extracted after the equations have been solved to give an explicit form for ψ that can then be mapped out in a two-dimensional contour plot.

The representation of ψ_1 must be made explicit. This is done through a Fourier series on an interval of horizontal length $2L$ centered about the leading edge of the cold air intrusion. Many convergence problems are avoided if the series is developed for functions that tend to zero at the end points of the interval. This can be achieved with the formulation

$$\psi_1(x, 0) = A[\tanh(x/h) - \sin(\pi x/2L)] + A \sin(\pi x/2L). \tag{12}$$

The term in brackets can be Fourier transformed on the interval, whereas the hyperbolic tangent alone may not be so treated. So we obtain a series that starts with the subharmonic:

$$\psi_1(x, 0) = A \sum_j F_j \sin(j\pi x/L). \tag{13}$$

The index j runs over the sequence (½, 1, 2, 3, . . . , N, . . .),

$$F_{1/2} = 1 \tag{14}$$

and

$$F_N = \frac{1}{L}\int_{-L}^{L} dx[\tanh(x/h) - \sin(\pi x/2L)] \sin(N\pi x/L). \tag{15}$$

All series developed on this pattern are found to converge properly.

Then in the full (x, z) plane

$$\psi_1(x, z) = \sum_j \phi_j(z) \exp(ik_j x) + \text{complex conjugate} \tag{16}$$

where

$$k_j = j\pi/L \tag{17}$$

and the ϕ_j must be found by solving the equations subject to all the boundary conditions.

This complex representation allows the governing equations (7), (9) to be separated into equations for each Fourier component:

$$\frac{d^2}{dz^2}\phi_j - (\bar{\rho}'/\bar{\rho})\frac{d}{dz}\phi_j + Q(z)\phi_j = 0 \tag{18}$$

$$Q(z) = \begin{cases} (N^2/U^2 - k_j^2) & \text{uppermost region} \\ (N^2/U^2 - U''/U - k_j^2) & \text{middle layer} \\ (-k_j^2) & \text{surface layer} \end{cases} \tag{19}$$

and the prime continues to represent a derivative with respect to z.

The term $(\bar{\rho}'/\bar{\rho})$ in (18) introduces the density weighting factor $\bar{\rho}^{1/2}$ into the solution ϕ_j, as is well known from internal gravity wave theory (Appendix). But for many problems, including the one of present concern, nothing important is lost when the coefficient $(\bar{\rho}'/\bar{\rho})$ is replaced by its average value within the layer

$$\langle \bar{\rho}/\bar{\rho}' \rangle_{\text{layer}} = -H_{\text{layer}} \tag{20}$$

so that (18) reduces to the simpler form

$$\frac{d^2}{dz^2}\phi_j + \frac{1}{H}\frac{d}{dz}\phi_j + Q(z)\phi_j = 0. \tag{21}$$

Equation (21), rather than (18), is used in all calculations. It simplifies the representation of ϕ_j, without modifying the qualitative results of the model. It is unlikely that the model is even modified quantitatively to any significant degree by this approximation.

The solution ϕ_j now has a simple form in two of the layers. In the uppermost layer

$$\phi_j = c_j \exp\{\pm z[N^2/U^2 - k_j^2 - 1/(4H^2)]_\infty^{1/2}\} \tag{22}$$

where the sign of the radical must be chosen so that the group velocity of the wave is directed upward. At this point the amplitude c_j is unknown. In the lowermost layer

$$\phi_j = \frac{A}{2i} F_j[a_j \exp[z(k_j^2 + 1/4H^2)^{1/2}] + (1 - a_j)\exp[-z(k_j^2 + 1/4H^2)^{1/2}]. \tag{23}$$

Again, a_j is presently unknown, but the combination of the linearly independent solutions of (21) has been selected so that the condition (13) is automatically satisfied. This is easily seen. Set $z = 0$ in (23) to obtain $\phi_j(0)$, and use the result in (16) for $z = 0$. It is immediately found that the desired form (13) is regained.

In the intermediate layer ϕ_j must generally be determined numerically. It is now observed that this solution in the intermediate layer must obey two boundary conditions at each of its interfaces with the adjacent layers. These boundary conditions are that pressure and displacement must be continuous across these interfaces. But four linearly independent conditions imposed on a second-order differential equation represent two excess constraints, or overdeterminances. These excess constraints thus determine c_j and a_j of (22) and (23). It is a relatively straightforward task to provide a numerical code that yields these amplitudes, and consequently the entire solution $\phi_j(z)$.

5. Results and discussion

We now present some results of the model calculations. It was found that in all the flows studied, the Fourier series converged satisfactorily. Usually about 50 terms were retained in the integer part of the sequence j [Eq. (13)]. This represented a considerable overkill as only the first half or less of them had significant amplitudes.

The first model inflow studied is shown in Fig. 4. Over most of the troposphere its temperature is similar to that shown in Fig. 1 for the rainband. At 9 km altitude, it is capped with a constant Brunt–Väisälä frequency of small magnitude. The wind is shown in the frame of reference for which the rainband is stationary. It is evident that it nowhere matches the rainband propagation speed and consequently excludes a steering level for the storms. This is deliberate. The model is to be compared with another that has a realistic wind profile. The dynamics of the two flows are very different.

The shape of the intrusion is deduced from the geometry of the upstream surface streamline. Once the ϕ_j are all obtained, the series (16) yields the value of streamfunction component ψ_1 throughout the (x, z) domain. The mean component $\bar{\psi}$ is defined by the upstream flow field, [see (4), (6)] and is thus known at the outset. Then the total streamfunction

$$\psi(x, z) = \psi_1(x, z) + \bar{\psi}(z) \tag{24}$$

is loaded on a two-dimensional array of grid points covering the domain of the computations and contoured using a standard graphics code. The resulting plots, contours of constant ψ, are the streamlines of the flow. The lowermost physical streamline defines the shape of the intrusion. Figure 6 shows the shape derived by this method. Note how the upstream ground-level streamline rises sharply to define the leading edge of the intrusion, overshoots in the head region, and settles back to an almost constant level above the ground to define the region taken over by

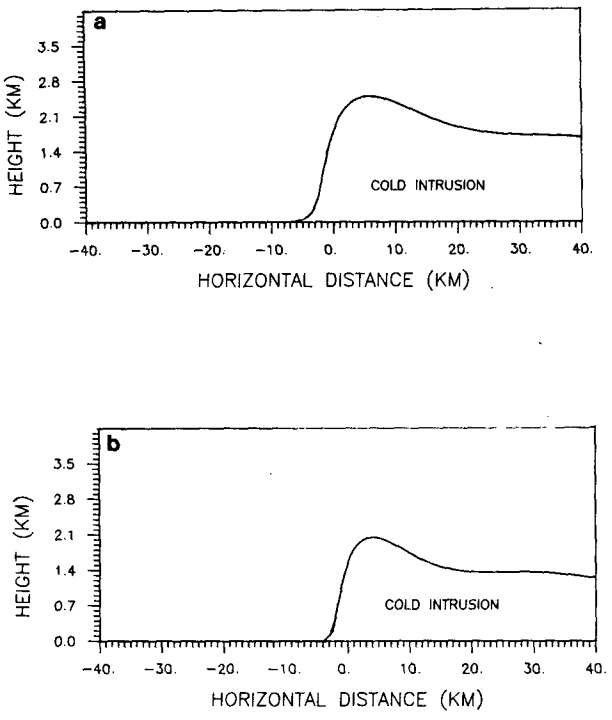

FIG. 6. Cold air current shapes defined by streamlines that start at ground level in the upstream flow. (a) Results from the flow set of Fig. 4, and the scale $2h = 1700$ m for the intrusion [Eq. (10)]; (b) results when the wind shear in the upper region is halved, and $2h$ is reduced to 1400 m.

the cold air intrusion. Figure 6 provides as realistic a shape for the cold air intrusion as we could wish at this time. We have experimented with various upper-level flows, but the shape of the lowest streamline always retains the same characteristics.

The stability of the flow is examined by plotting tephigrams on vertical sections above selected ground sites. Figures 7a–d show a sequence of these along the same model flow that produced the intrusion shape of Fig. 6a. The horizontal location of each sounding is marked on Fig. 8. The moist adiabats usually shown have been suppressed, except for the section indicated by the overdotted line. This is a continuation of the sounding provided by the saturated boundary layer. The first sounding, Fig. 7a, shows the inflow used. It indicates parcel stability in the upstream region. However, as the flow encounters the intrusion, considerable thermal instability is generated (Fig. 7b–d). The origin of this instability is clear. The saturated boundary layer air follows wet adiabats, while the air above it follows dry adiabats. This difference in (T, θ) curves is most apparent at the interface of the two air layers, where it produces a convectively unstable temperature discontinuity. More realistically, this temperature drop would be distributed over a transition layer. It is not too difficult to interpolate the transition region from the flow calculated here and the inflow humidity profile. But in view of the findings to be subsequently reported for the realistic wind, this will not be pursued. Note that all parcels in the saturated region behind the intrusion now have positive area for lifting.

These tephigrams indicate potential instability (i.e., conditional and convective instability together) that would be expected to drive deep cellular convection. In particular, Fig. 7c shows a positive area for lifting up to the 325-mb level (approximately 10-km altitude). The rainband does not contain such convection, and we will see that the stability patterns of the more realistic model used next are quite different.

The total flow pattern over the intrusion is shown in Fig. 8. Its resemblance to the lee wave flow over a ridge is apparent. However, this suggests that a number of results from lee wave studies may be applicable to these surface intrusions. For instance, the severity of the instability in the lifted air mass depends on the strength of upper-level displacement as it mounts the cold air intrusion. This displacement can be enhanced by particular combinations of upper-air wind and temperature profiles. Most obviously, if the flow supports a natural mode that has the same phase speed as the cold-air current, a resonant response of the type that dominates lee waves can be expected. The severity of the response to a cold air intrusion must reflect such effects.

We now turn to a model using more realistic profiles. Figure 5 shows an inflow fitted to rainband data. Our integration routines are more efficient when supplied with analytical expressions rather than data sets and interpolation procedures. Thus the profiles used are constructed from standard functions.

The major difference between this inflow and the one used previously is the steering level in the midtroposphere; it shows up in the working frame of reference as a zero of the mean wind. The data do not determine the altitude of the steering level very accurately, so we ran several models that bracket the allowed range. The general behavior of all of them is much the same, and only one set of results will be reported.

We now encounter a mathematical complication. All the functions ϕ_j in (16) contain a singular critical level—the height at which U is zero and Q of (19) becomes infinite. This singularity is negotiated using Frobenius expansions (Appendix). Otherwise the numerical procedures are unchanged.

Figures 9 and 10 show the flow field that results. The intrusion has the same shape as before, but the flow above it is different. The dynamic response in the lifted air is so strong that there are flow reversals and regions of unstable temperature gradients. It was to be expected that the flow near the critical level would be untenable. But these calculations indicate a breakdown of the laminar flow through much of the midtroposphere.

The results may be interpreted in the framework of wave theory where considerable research has been devoted to such flow breakdown (Hodges, 1967; Lindzen,

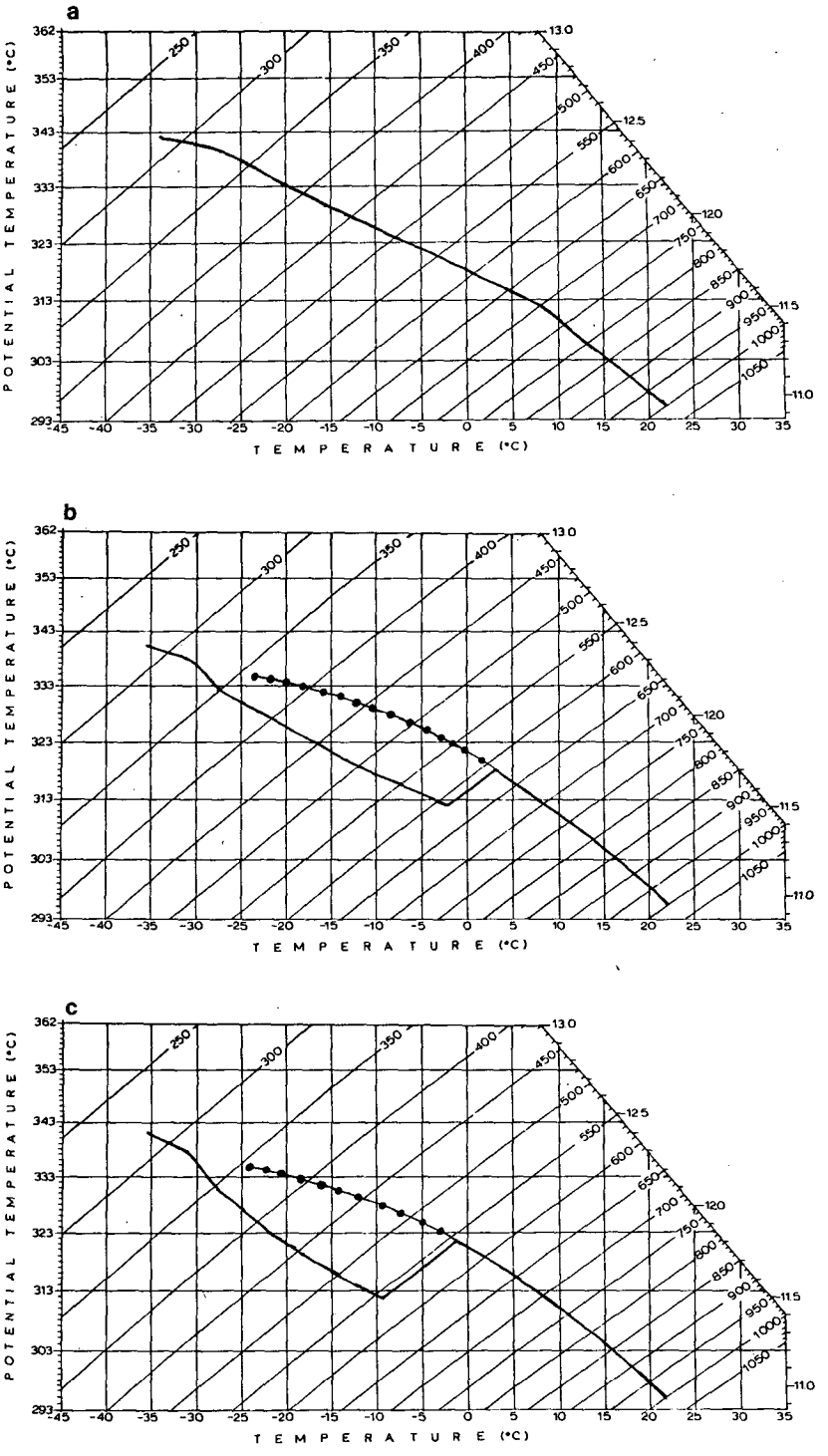

FIG. 7. Tephigrams "soundings" when the inflow of Fig. 4 encounters the intrusion. Horizontal locations of "soundings," marked in Fig. 8, range from (a) far upstream to (d) far downstream, while maximum lifting occurs near (c). The heavily dotted line is the saturated adiabat that would be followed by a parcel lifted out of the saturated layer.

1981, Lindzen and Forbes, 1983; Orlanski and Ross, 1973; Fritts, 1984). The linearized response calculated for the unsaturated region can be accepted in regions where it is self-consistent. This requires that density and pressure "perturbations" are less than the mean values, and that the assumption of stationarity is not

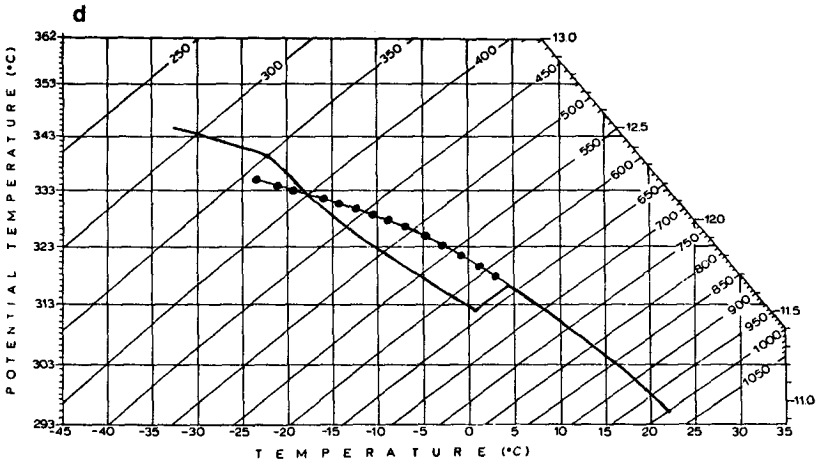

FIG. 7. (*Continued*)

violated. This latter condition demands that the velocity perturbation cannot reverse the flow in any streamtube. All three conditions are often violated simultaneously, as is the case here. It is believed that in such circumstances the "wave" forces a convective overturning of the local fluid, with an accompanying loss of energy from the wave field.

At this stage we do not attempt to model or parameterize the nonlinear interactions involved. It is not even clear that this is feasible. Nevertheless, the generally expected result will be a flow pattern something like Fig. 11. The flow is laminar where the linearized theory is consistent and turbulent where it first breaks down. Absorption of the wave limits its amplitude in the downstream regions, which are laminar again. The steering level caps the response region, there being essentially no wave penetration above this height.

The expected behavior with respect to moist instability and severe convection is not at all obvious in such complicated circumstances, although some general features are evident. Foremost, the convective instability is generated between the saturated surface layer and the overlying air exactly as in the first model. The

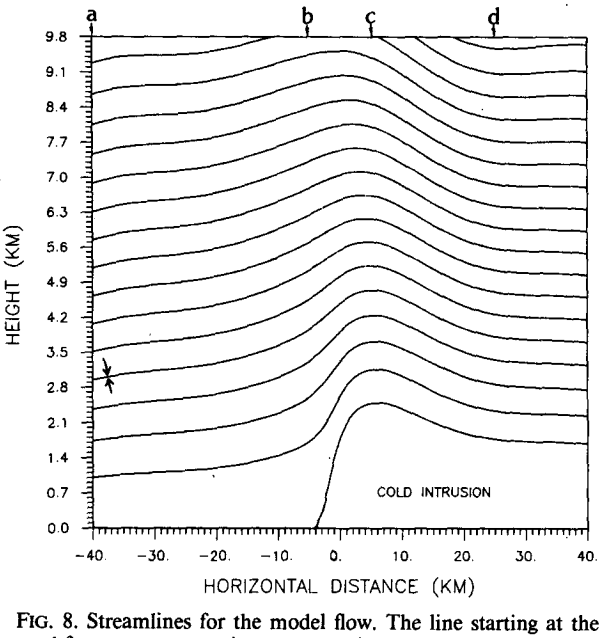

FIG. 8. Streamlines for the model flow. The line starting at the ground far upstream remains at ground level till it rises abruptly at −4 km to define the boundary of the cold intrusion. The streamline indicated by the arrows is the upper surface of the saturated layer.

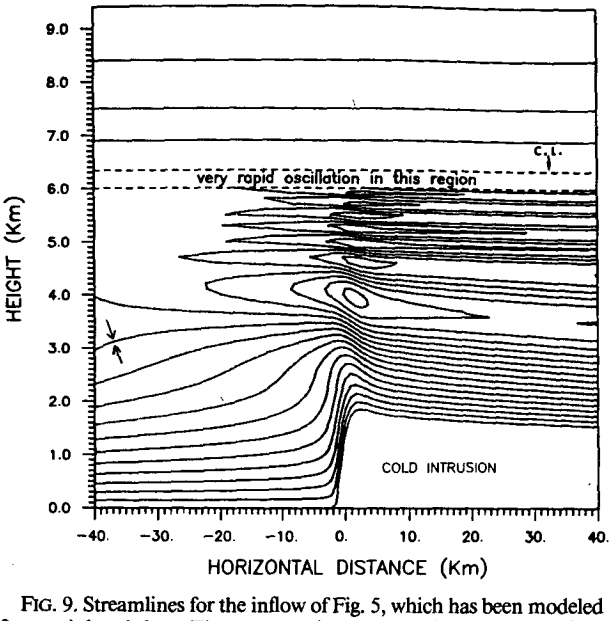

FIG. 9. Streamlines for the inflow of Fig. 5, which has been modeled from rainband data. The response is so strong that regions of flow reversal have developed. These connect to return flows of the "correct" sign, but such streamlines produce unstable density structure. Above the steering (critical) level the response is negligible. The streamline indicated by the arrows is the upper surface of the saturated layer.

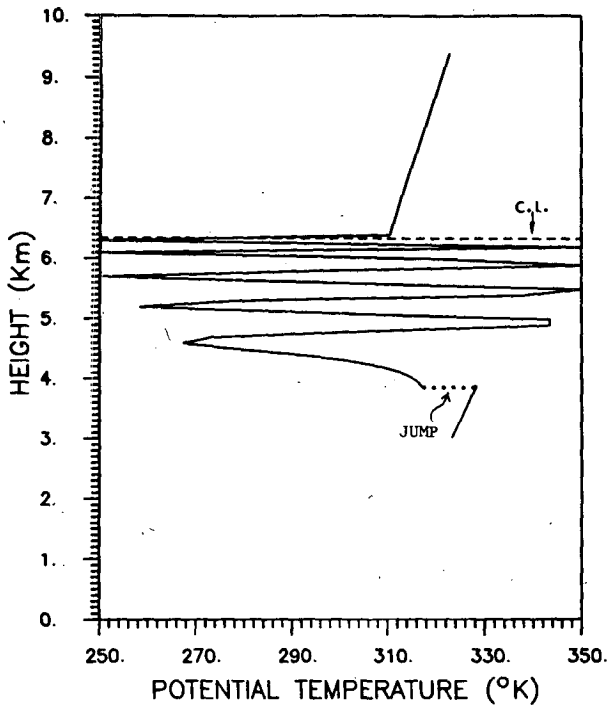

FIG. 10. Sounding for the flow of Fig. 9 in a vertical section at the head of the intrusion. The jump discontinuity marks the interface of the saturated layer with the overlying dryer region. A region in which potential temperature decreases with height is statically unstable.

temperature drop at the interface of the layers is shown as the "jump" in Fig. 10. It now underlies a region of decreasing potential temperature generated by the dynamic response in the unsaturated layer. Severe convection must be expected, but difficulties arise when we attempt to estimate the expected depth of the convection.

We cannot draw tephigrams and discuss their positive areas for lifting in the conventional manner because the profiles are most unconventional. (Figure 10 for the potential temperature through the unsaturated region above the head of the intrusion has already indicated this.) The potential temperature is not a monotonically increasing function of height, and its reversals make the tephigrams undecipherable. Instead we will use the potential temperature plot directly to discuss the convective response.

Figure 10 indicates convective instability above the cold air intrusion up to a height of about 4.5 km. This altitude range should contain severe moist convection. The plot then shows an alternating stucture of inversions and convectively unstable regions up to the critical level at 6.3 km, and above this height an undisturbed atmosphere. We recognize that the convectively unstable regions will be turbulent. But we cannot estimate whether this turbulence will penetrate the intervening inversions to form one continuously turbulent region, or whether alternating layers of laminar and turbulent atmosphere should be expected. Likewise, we do not know if the severe moist convection produced below 4.5 km will penetrate the inversion just above and merge into the overlying turbulence. It is clear that this model does not give the straightforward prediction of deep cellular convection obtained in the earlier model. However, it has also led to a stability situation for which there is no conventional interpretation. As such it is probably best to avoid further speculation and compare the model results with the observed situation.

Observation of rainbands shows that severe convection is confined to relatively shallow layers. In the study reported by Carbone (1982), the data indicate an upper level for recognizable rainband activity that is close to 6.5 km. This is consistent with the height of the steering level, and hence the height predicted here for a return to a laminar flow essentially devoid of any wave activity. Perhaps this is coincidence. Nevertheless, we tentatively postulate that it is causal, with the rainband location determined by the region of strong wave activity. There is the further possibility that severe convection is confined to a lower region within the rainband, identified in the model by the lowest inversion in the flow field. This is not inconsistent with the observations, but more detailed field studies are needed to determine if there is some separation into a lower level dominated by moist convection and an upper level (or levels) where turbulence is the major element in the activity.

We will draw one final concept from the lee wave analogy. In this work we have dealt with the mature

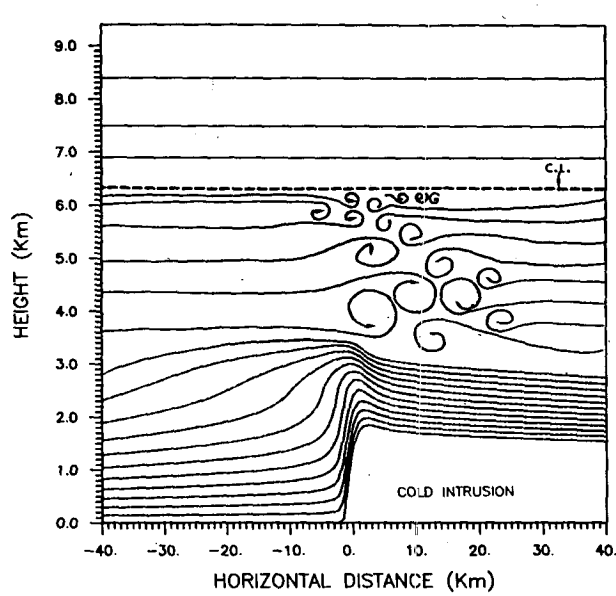

FIG. 11. Schematic of possible flow when overturning and turbulence are taken into account for the system represented previously in Fig. 9. Outflow has correct sign, and downstream wave amplitude is much reduced by wave absorption in the overturning fluid.

line and have not questioned how it first develops or what selects its orientation. Atmospheric wave theory recognizes that the response to any disturbance is usually dominated by modal components. The atmospheric modes display anisotropy introduced by the mean wind structure. That is, the modes have preferred orientations in the horizontal plane. This anisotropy could play a major part in selecting the orientation of the rainband and guiding its development into a mature two-dimensional structure from initially localized disturbances.

Acknowledgments. We gratefully acknowledge help received from R. E. Carbone and J. A. Moore who provided information and data from their studies of the California severe rainband of 5 February 1978. Results from this study are included in the Ph.D. thesis of G. Kallos, submitted to the School of Geophysical Sciences, Georgia Institute of Technology, 1985. This work was partially supported by the National Science Foundation under Grant ATM8217152, and the University of Athens who funded the first year of G. Kallos's stay in the United States.

APPENDIX

An Outline of the Wave Formulas

1. Equations of motion in the saturated layer

The equations governing the steady state two-dimensional saturated flow may be written

$$\mathbf{V}\cdot\nabla\mathbf{V} = -\frac{1}{\rho}\nabla p + \mathbf{g}, \tag{A1}$$

$$\nabla\cdot(\rho\mathbf{V}) = 0, \tag{A2}$$

$$\rho = f(p). \tag{A3}$$

The first is Euler's equation and the second is the equation for conservation of mass. The third is the special form taken for an equation of state when all fluid elements in the layer are thermodynamically equivalent. Here θ_e is constant through the layer, so we have an extension from the more familiar isentropic gas system to one that allows for phase changes.

For a two-dimensional velocity field obeying (A2), a little vector analysis verifies the result

$$\nabla\times[\mathbf{V}\cdot\nabla\mathbf{V}] = \rho(\mathbf{V}\cdot\nabla)\frac{1}{\rho}\nabla\times\mathbf{V}. \tag{A4}$$

But since the flow is stationary, the advective derivative D/D_t reduces to $(\mathbf{V}\cdot\nabla)$ alone, and (A4) can be rewritten as

$$\nabla\times[\mathbf{V}\cdot\nabla\mathbf{V}] = \rho\frac{D}{Dt}\left(\frac{1}{\rho}\nabla\times\mathbf{V}\right). \tag{A5}$$

The special equation of state that holds here causes the right-hand side of (A1) to be irrotational since

$$\frac{1}{\rho}\nabla p = \frac{1}{f(p)}\nabla p = \nabla P(z) \tag{A6}$$

where

$$P = \int^{p(z)}\frac{1}{f(p')}\,dp'. \tag{A7}$$

Consequently, taking the curl of (A1) we obtain

$$\nabla\times[\mathbf{V}\cdot\nabla\mathbf{V}] = \nabla\times[-\nabla P + \mathbf{g}] \equiv 0, \tag{A8}$$

and with (A5) this provides the result

$$\frac{D}{Dt}\left(\frac{1}{\rho}\nabla\times\mathbf{V}\right) = 0. \tag{A9}$$

This states that $\rho^{-1}\nabla\times\mathbf{V}$ is advected without change, and thus retains its upstream inflow value along a given streamline. In the notation of the density weighted streamfunction of section 3,

$$\frac{D}{Dt}\left(\frac{1}{\rho}\nabla\cdot\frac{1}{\rho}\nabla\psi\right) = 0 \tag{A10}$$

so

$$\frac{1}{\rho}\nabla\cdot\frac{1}{\rho}\nabla\psi = \text{its value at the upstream inflow} = \frac{1}{\rho_0}\frac{du_0}{dz_0}, \tag{A11}$$

which gives us Eq. (3) of section 3.

2. Wave equation in the unsaturated medium

The time-independent linearized equations in the unsaturated layers are taken to be

$$\rho_0(\mathbf{U}\cdot\nabla\mathbf{V}_1 + \mathbf{V}_1\cdot\nabla\mathbf{U}) = -\nabla p_1 + \rho_1\mathbf{g}, \tag{A12}$$

$$\nabla\cdot\mathbf{V}_1 = 0, \tag{A13}$$

$$\mathbf{U}\cdot\nabla\rho_1 = -N^2w_1\rho_0/g, \tag{A14}$$

$$\mathbf{V}_1 \equiv \hat{x}u_1 + \hat{z}w_1,$$

where U, the mean flow velocity, is a function of z only, and the disturbances are functions of x and z only. Conservation of mass has been approximated with the divergence-free condition, and a term in p_1 has been dropped from the equation of state (A14). These approximations are not essential to the analysis, but the full algebraic development (e.g., Chimonas, 1970) only introduces corrections that are of relative magnitude (wave phase speed/speed of sound)^2 and these are not significant in the present study.

The four linear equations (A12)–(A14) in the four scalar field components can be manipulated with straightforward algebra into the second-order differential Eq. (9) of section 3.

3. Density weighting factors and upper-boundary conditions

The internal gravity wave obeys an equation of the general form

$$\frac{d^2y}{dz^2} \pm (\rho_0'/\rho_0)\frac{dy}{dz} + Q(z)y = 0 \qquad \text{(A15)}$$

[cf. (18) of text], where the choice $\pm$ depends on the field component being studied. The first-order derivative can be removed with the canonical transformation

$$y = \rho_0^{\mp 1/2} q \qquad \text{(A16)}$$

$$\frac{d^2q}{dz^2} + [Q(z) \pm \rho_0''/2\rho_0 + (\rho'/2\rho_0)^2]q = 0. \qquad \text{(A17)}$$

The density weighting factor $\rho_0^{\pm 1/2}$ seen in (A16) causes the wave amplitudes for velocity and relative density and relative pressure to grow as the wave propagates into the lower densities of the upper atmosphere. The additional terms that now modify $Q(z)$ in (A17) involve only the local density scale height H and its first derivative. An order of magnitude estimate shows that variations in H contribute very small corrections to the equations, which is why we replaced the factor $\bar{\rho}'/\bar{\rho}$ in (18) with a layer-averaged value.

In the uppermost layer of all the model calculations wind and stratification are made constants so that the coefficients of (A17) are constants. This provides for pairs of exponential solutions to the equation. If the coefficient multiplying q is negative the exponentials are real and one decays as z increases towards infinity, while the other grows without limit. Only the former behavior is physically acceptable so the solutions from the lower regions must be matched to the decaying form where the uppermost layer begins. If the coefficient is positive the exponentials are wave-like, and one corresponds to upward propagation of energy and group velocity from a source in the lower levels, while the other corresponds to a generation mechanism at infinite z (Hines, 1960). Again, only the former behavior is physically acceptable, so the disturbance must be matched to this wave at the boundary where the uppermost layer begins.

4. The Frobenius expansion

The equation

$$\frac{d^2\phi}{dz^2} - (\bar{\rho}'/\bar{\rho})\frac{d\phi}{dz} + \left(\frac{N^2}{U^2} - \frac{U''}{U} - k^2\right)\phi = 0 \qquad \text{(A18)}$$

is singular at a point z_c where U is zero. This is a so-called critical level, and of course the computer cannot integrate through it. Instead we must supply a procedure that bridges z_c.

A regular Taylor series about z_c is no more possible than a direct integration through it, and for the same reasons. However, a modified series known as a Frobenius expansion can be used. The coefficients in the equation are written as expansions in $(z - z_c)$. For example,

$$\frac{N^2}{U^2} = \frac{N^2(z_c)\{1 + a_1(z - z_c) + a_2(z - z_c)^2 + \cdots\}}{[U'(z_c)(z - z_c) + b_2(z - z_c)^2 + \cdots]^2}, \qquad \text{(A19)}$$

$$= \left(\frac{N(z_c)}{U'(z_c)}\right)^2 \frac{1}{(z - z_c)^2} \times \{1 + c_1(z - z_c) + c_2(z - z_c) + \cdots\}. \qquad \text{(A20)}$$

We now seek the Frobenius expansion

$$\phi = \text{constant}\ (z - z_c)^\alpha\{1 + d_1(z - z_c) + d_2(z - z_c)^2 + \cdots\} \qquad \text{(A21)}$$

which is required to satisfy the differential equation in the sense that each power of $(z - z_c)$ in the expansion of (A18) will balance separately. This balance allows the coefficients in the Frobenius expansion to be calculated sequentially in much the same way as a Taylor series solution is found about a regular point. The only essential difference is that the balance of the leading order produces an algebraic expression for α. This generally allows two distinct noninteger values for α, and thus two distinct solutions of the form (A21). It is, of course, normal for a second-order differential equation to have two linearly independent solutions.

Using these two series, we can bridge the region about z_c with a small semicircle in the complex z plane (Booker and Bretherton, 1967) and so complete the integration of the equation over the entire range of z.

REFERENCES

Booker, J. R., and F. P. Bretherton, 1967: The critical layer for internal gravity waves in a shear flow. *J. Fluid Mech.*, **27**, 513–539.

Carbone, R. E., 1982: A severe frontal rainband. Part I: Stormwide hydrodynamic structure. *J. Atmos. Sci.*, **39**, 258–279.

Chimonas, G., 1970: The extension of the Miles–Howard theorem to compressible fluids. *J. Fluid Mech.*, **43**, 833–836.

Fritts, D. C., 1984: Gravity wave saturation in the middle atmosphere: A review of theory and observations. *Rev. Geophys. Space Phys.*, **22**, 275–308.

Hines, C. O., 1960: Internal gravity waves at ionospheric heights. *Can. J. Phys.*, **38**, 1441–1481.

Hobbs, P. V., and O. G. Persson, 1982: The mesoscale and microscale structure and organization of clouds and precipitation in midlatitude cyclones. Part V: The substructure of narrow cold frontal rain bands. *J. Atmos. Sci.*, **39**, 280–295.

Hodges, R. R., Jr., 1967: Generation of turbulence in the upper atmosphere by internal gravity waves. *J. Geophys. Res.*, **72**, 3455–3458.

Lilly, D. L., 1979: The dynamical structure and evolution of thunderstorms and squall lines. *Ann. Rev. Earth and Planet. Sci.*, **7**, 117–161.

Lindzen, R. S., 1981: Turbulence and stress due to gravity wave and tidal breakdown. *J. Geophys. Res.*, **86**, 9707–9714.

——, and J. Forbes, 1983: Turbulence originating from convectively stable internal waves. *J. Geophys. Res.*, **88**, 6549–6553.

Moore, J. A., 1986: The meso-synoptic environment of a severe winter cold frontal rainband. In preparation.

Orlanski, I., and B. B. Ross, 1973: Numerical simulation of the generation and breaking of internal gravity waves. *J. Geophys. Res.*, **78**, 8808–8826.